Drying with Internal Heat Generation: Theoretical Aspects and Application to Microwave Heating

T. Constant and C. Moyne
Laboratoire d'Energétique et de Mécanique Théorique et Appliquée, 54504 Vandoeuvre-Les Nancy, France

P. Perré
Ecole Nationale du Génie Rural et des Eaux et Forêts, 54000 Nancy, France

A model of simultaneous heat and mass transfer presented describes drying with internal heat generation. Since a liquid expulsion phase is observed, a numerical procedure was developed to account for saturated and unsaturated zones and to model the liquid expulsion. The model was validated by a drainage experiment. An experimental rig was built to conduct microwave drying experiments in well-controlled conditions using capillary porous body (light concrete) as test material. Two types of drying (high and low power) were distinguished, depending on whether or not boiling occurred in the sample. The heat source term in the medium was determined from the experimental results. The numerical results agree with the experimental observations in terms of drying kinetics and transfer mechanisms. This allows a very accurate description of the transport phenomena and the liquid expulsion phase associated with high-power drying.

Introduction

From a theoretical standpoint, drying is a simultaneous heat and mass transfer in porous media. A practical way to distinguish between the various drying methods is to classify them by heating mode: convective drying, external radiative drying, and conductive (contact) drying. Drying with internal heat generation, such as microwave drying, is a special case.

Microwave drying exploits the polarization of molecules (especially of polar water molecules), which are unable to follow extremely rapid reversals of high frequency electrical field to heat moist materials. Microwave radiations have typical centimetric or decimetric wavelengths and a penetration depth of roughly the same order of magnitude, commensurate with the size of the sample to be dried. For instance, the wavelength of an electromagnetic signal at frequency 2.45 GHz is 12.4 cm and the penetration depth, that is, the distance from the surface of the material at which the power drops to $e^{-1} = 0{,}63$ from its initial value, is 2 cm of water at 60°C. Thus, due to dielectric losses, as well as direct conductive effects, a volumic heat source is dissipated throughout the material.

Two different but interlinked problems need to be considered:

- Computation of the internal heat source due to electromagnetic radiation inside the medium
- Modeling of heat and mass transfer and of drying kinetics.

The electromagnetic problem is a challenge today and is not discussed here. Refer to Metaxas and Meredith (1988) for a general introduction to microwave heating. Some indications are provided elsewhere (Constant, 1992). In this article, the internal heat source is assumed to be known. More precisely, an average value of the heat source is available from experimental data, and an appropriate procedure is used to estimate its spatial distribution.

The objective of this article is to understand the second problem, that is, the detailed physical mechanisms which occur during drying with internal heat sources. First, heat-and mass-transfer theory, discussed at length in a previous article (Moyne and Perré, 1991) is briefly reviewed. The set of partial differential equations is derived at the macroscopic level using phenomenological relations for the flux constitutive equations. This intuitive approach can be justified from the theoretical standpoint by integrating the equations at the pore level over the so-called representative elementary volume in order to obtain the macroscopic formulation (Whitaker, 1977).

A number of assumptions are necessary to keep the system in a tractable form. The medium is assumed to be in local thermodynamic equilibrium. This hypothesis, in connection with microwave drying of brick, was examined by Jolly and

Turner (1990) who concluded that no significant differences occur between the average temperatures of each phase during dielectric heating.

Close attention is paid to the role of the total gaseous pressure gradient as an additional driving force in both the gas phase and liquid phases. This agrees with the previous work of Moyne (1987) and Perré (1987) concerning high- and low-temperature convective drying. When the temperature of the medium exceeds the boiling point imposed by the external pressure, the total gaseous pressure gradient acting on both gas and liquid phases becomes the major driving force. This situation is referred as "high-temperature" drying. The other case, where drying proceeds by evaporation (as opposed to vaporization), is referred to as "low-temperature" drying.

Another special point developed here concerns the simultaneous description of both a saturated and an unsaturated zone inside the medium and the process of liquid expulsion. In dielectrically enhanced drying, a *liquid movement period* can be observed for high power density and media which contain large amounts of liquid. This was observed by many researchers (Lyons et al., 1972; Lefeuvre et al., 1978; Morrow (1980) and corresponds to a high drying rate with concomitant energy savings. The material surface becomes wet, liquid may flow in a thin film, and drops may even be expelled. This mechanism is exploited for the renovation of historic monuments though the microwave drying of washed stones. In this case, the previous formulation fails because of the absence of a gas phase. A specific experiment is conducted to test the validity of the macroscopic formulation in this case.

An experimental rig was built for a microwave drying system. It consists of a large wave-guide in which a cylinder of aerated concrete is positioned transversally.

The final portion of this article compares the experimental and theoretical results. Four periods were observed for both results, which showed good agreement. This allowed a very detailed description of the physical mechanisms occurring during microwave drying.

Theory

The porous medium is assumed to be rigid and to contain three phases: solid (s), liquid (l) and gas (g). The gas phase has two components: water vapor (v) and air (a).

Mass balances

The macroscopic mass balance for the liquid phase, and for water vapor and air in the gas phase, are written:

Liquid phase

$$\rho_0 \frac{\partial X_1}{\partial t} + \nabla \cdot \boldsymbol{n}_1 = -\dot{m} \tag{1}$$

with

$$\boldsymbol{n}_1 = \rho_1 \boldsymbol{u}_1 \tag{2}$$

Water vapor

$$\rho_0 \frac{\partial X_v}{\partial t} + \nabla \cdot \boldsymbol{n}_v = \dot{m} \tag{3}$$

with

$$\boldsymbol{n}_v = \rho_v \boldsymbol{u}_v = \rho_v \boldsymbol{u}_g + \boldsymbol{j}_v \tag{4}$$

Air

$$\rho_0 \frac{\partial X_a}{\partial t} + \nabla \cdot \boldsymbol{n}_a = 0 \tag{5}$$

with

$$\boldsymbol{n}_a = \rho_a \boldsymbol{u}_a = \rho_a \boldsymbol{u}_g + \boldsymbol{j}_a \tag{6}$$

where $\dot{m}$ is the phase change term (that is, the mass of evaporated water per unit volume of porous medium and per unit time).

The water vapor (respectively air) mass flux is the sum of a convective term with the gas superficial velocity $\boldsymbol{u}_g$ and a diffusive term $\boldsymbol{j}_v = -\boldsymbol{j}_a$ where $\boldsymbol{j}_v$ is the diffusive mass flux of air and vapor relative to the mass averaged velocity of the gas phase $\boldsymbol{u}_g$.

Energy balance

Ignoring kinetic energy and pressure terms which are usually unimportant, the energy balance is obtained as:

$$\rho_0 \frac{\partial}{\partial t}\left(h_s + \int_0^{X_1} h_1 dX_1 + X_v h_v + X_a h_a\right) = -\nabla \cdot (\boldsymbol{q} + h_1(X_1)\boldsymbol{n}_1 + h_v \boldsymbol{n}_v + h_a \boldsymbol{n}_a) + \Phi \tag{7}$$

where $h_i (i = a, l, s, v)$ denotes the mass enthalpy of component i; for air and water vapor (ideal gases) and for solid phase, the enthalpy is assumed to depend only on temperature; for liquid phase, it is assumed to depend both on temperature and moisture content. $\boldsymbol{q}$ is the heat flux density and Φ is the heat source term.

By writing the enthalpy term for liquid water, the integral sign is used as a reminder that bound water (contrary to free water) does not form a single phase.

The use of conservation Eqs. 1, 3, and 5 leads to:

$$\rho_0\left(\frac{\partial h_s}{\partial t} + \int_0^{X_1} \frac{\partial h_1}{\partial t} dX_1 + X_v \frac{\partial h_v}{\partial t} + X_a \frac{\partial h_a}{\partial t}\right) + (\boldsymbol{n}_1 \cdot \nabla h_1(X_1) + \boldsymbol{n}_v \cdot \nabla h_v + \boldsymbol{n}_a \cdot \nabla h_a) = -\nabla \cdot \boldsymbol{q} - \Delta h_v \dot{m} + \Phi \tag{8}$$

where $\Delta h_v = h_v - h_1$ is the latent heat of vaporization of water. If the water is absorbed, it includes the differential heat of sorption.

Introduction of the specific heat capacity at constant pressure (and assuming it to be constant for absorbed water) leads to:

$$\rho_0 c_p \frac{\partial T}{\partial t} + (\rho_1 c_{pl} \boldsymbol{u}_1 + \rho_v c_{pv} \boldsymbol{u}_v + \rho_a c_{pa} \boldsymbol{u}_a) \cdot \nabla T + \rho_1 \left(\frac{\partial h_1}{\partial X_1}\right) \boldsymbol{u}_1 \cdot \nabla X_1 = -\nabla \cdot \boldsymbol{q} - \Delta h_v \dot{m} + \Phi \tag{9}$$

where $c_p = c_{ps} + X_l c_{pl} + X_v c_{pv} + X_a c_{pa}$ is the specific heat capacity of the material being dried per unit mass of dry solid.

Phenomenological relations

In order to complete the system of equations, the expressions for the liquid mass flux $\boldsymbol{n}_l$, the gas mass flux $\boldsymbol{n}_g$ and for the gas diffusive flux $\boldsymbol{j}_v$ and the heat conduction flux $\boldsymbol{q}$ are required.

For the superficial average velocity of the liquid phase $\boldsymbol{v}_g$, the generalized Darcy's law is used:

$$\boldsymbol{u}_l = -\frac{\boldsymbol{K}\boldsymbol{k}_{rl}}{\mu_l}\cdot(\nabla P_l - \rho_l \boldsymbol{g}) \tag{10}$$

$$\boldsymbol{u}_g = -\frac{\boldsymbol{K}\boldsymbol{k}_{rg}}{\mu_g}\cdot(\nabla P_g - \rho_g \boldsymbol{g}) \tag{11}$$

Introducing an empirical resistance factor to gaseous diffusion through the porous medium f, the diffusive mass flux density of vapor $\boldsymbol{j}_v$ relative to the mass average velocity is written:

$$\boldsymbol{j}_v = -\boldsymbol{j}_a = -\rho_g D_v \boldsymbol{f}\cdot\nabla\left(\frac{\rho_v}{\rho_g}\right) \tag{12}$$

where D_v is the binary air-water vapor diffusion coefficient.

Fourier's law is used to write the heat flux density through the porous medium:

$$\boldsymbol{q} = -\boldsymbol{\lambda}\cdot\nabla T \tag{13}$$

The thermal conductivity tensor $\boldsymbol{\lambda}$ takes account of conductive heat transfer through a three-phase material as well as the increased heat transfer due to the local evaporation-condensation mechanism (Azizi et al., 1988; Moyne et al., 1988).

Equilibrium relations

The pressure differential between the gas and liquid phases, that is, the capillary pressure $P_c = P_g - P_l$, is assumed to depend only on the temperature and the liquid saturation (or the liquid moisture content):

$$P_g - P_l = P_c(T, X_l) \tag{14}$$

Thermodynamic equilibrium is assumed due to the long contact time between the phases. Hence the intrinsic average temperature of each phase is the same and the vapor pressure in the medium is given by the sorption equilibrium relations:

$$\frac{P_v}{P_{vs}} = \varphi(T, X_l) \tag{15}$$

System of equations to be solved

What is the number of unknowns necessary to determine the local state of the medium at the macroscopic level? One unknown is needed to describe how the liquid and the gas phases occupy the pore space. The state of the rigid solid phase is determined solely by the solid temperature. The liquid phase is described by two unknowns, for example, the liquid gas pressure and the liquid temperature. The gas phase (two components: air and water vapor) needs three parameters: for example, the gas temperature, the gas pressure, and the vapor concentration defined by the vapor pressure. Therefore, seven unknowns are needed. Assuming local thermal equilibrium (the temperatures of all three phases are identical), capillary equilibrium (Eq. 14) and liquid-vapor equilibrium (Eq. 15), this number is reduced to three.

Among the many choices of three independent variables, the temperature T, moisture content X ($X = X_l + X_v \cong X_l$), and total pressure in the gas phase P_g are selected. The choice of T and P_g is quite natural because the gradients of these two variables appear as the driving forces in Eqs. 10 and 13. The choice of X (rather than P_l, for example) is explained by the fact that X is the variable of practical interest and also allows easier calculation of the volume occupied by each phase.

The total mass-transfer equation is obtained by adding the conservation Eqs. 1 and 3 and by using Darcy's generalized law (Eqs. 10 and 11) and Fick's law (Eq. 12). Thus:

$$\frac{\partial X}{\partial t} = \nabla\cdot(\boldsymbol{D}_X\cdot\nabla X + \boldsymbol{D}_T\cdot\nabla T + \boldsymbol{D}_P\cdot\nabla P_g - \boldsymbol{D}_G\cdot\boldsymbol{g}) \tag{16}$$

The righthand side of Eq. 16 shows a diffusion-like term, a thermomigration term and a filtration term due to the total pressure in the gas phase and the gravitational acceleration. Note that each of these phenomenological coefficients $\boldsymbol{D}_X(=\boldsymbol{D}_X^l + \boldsymbol{D}_X^V)$, $\boldsymbol{D}_T = (\boldsymbol{D}_T^l + \boldsymbol{D}_T^v)$, $\boldsymbol{D}_P = (\boldsymbol{D}_P^l + \boldsymbol{D}_P^V)$, $\boldsymbol{D}_G = (\boldsymbol{D}_G^l + \boldsymbol{D}_G^v)$ is the sum of the contribution of both the liquid and gas phases.

The heat balance Eq. 9 is thus written:

$$\rho_0 c_p\frac{\partial T}{\partial t} + \rho_0\Delta h_v\frac{\partial X_v}{\partial t} + (c_{pl}\boldsymbol{n}_l + c_{pv}\boldsymbol{n}_v + c_{pa}\boldsymbol{n}_a)\cdot\nabla T + \left(\frac{\partial h_l}{\partial X_l}\right)_T \boldsymbol{n}_l\cdot\nabla X_l = \nabla\cdot(\boldsymbol{k}\cdot\nabla T + \rho_0\Delta h_v\boldsymbol{D}_X^v\cdot\nabla X + \rho_0\Delta h_v\boldsymbol{D}_P^v\cdot\nabla P_g) \tag{17}$$

where $\boldsymbol{k} = \boldsymbol{\lambda} + \rho_0\Delta h_v\boldsymbol{D}_T^v$ is the apparent thermal conductivity of the medium.

Finally, the air mass balance is written:

$$\alpha\frac{\partial P_g}{\partial t} - \beta\frac{\partial X}{\partial t} - \gamma\frac{\partial T}{\partial t} = \nabla\cdot(-\boldsymbol{D}_T^v\cdot\nabla T - \boldsymbol{D}_X^v\cdot\nabla X + \boldsymbol{D}_P^a\cdot\nabla P_g) \tag{18}$$

The exact expression of these terms is given in the Appendix. The system to be solved is a set of three partial derivative Eqs. 16, 17, and 18.

Boundary conditions

If the porous medium at the interface is not saturated in case of drying at atmospheric pressure P_{atm}, the lost mass

flux density ϕ_m at the interface and the heat flux density ϕ_h given by the surroundings are written:

$$\phi_m = (\boldsymbol{n}_l + \boldsymbol{n}_v)\cdot\boldsymbol{n}_{ext}$$
$$= -\rho_0(\boldsymbol{D}_X\cdot\nabla X + D_T\cdot\nabla T + \boldsymbol{D}_P\cdot\nabla P_g - \boldsymbol{D}_G\cdot\boldsymbol{g})\cdot\boldsymbol{n}_{ext} \quad (19)$$

$$\phi_h = (-\boldsymbol{q} - (h_l\boldsymbol{n}_l + h_v\boldsymbol{n}_v) + h_v(\boldsymbol{n}_l + \boldsymbol{n}_v))\cdot\boldsymbol{n}_{ext} \quad (20)$$

where $\boldsymbol{n}_{ext}$ is the normal outwardly directed to the medium.

The combination of the above two equations and the use of phenomenological equations instead of Eq. 20 leads to:

$$-(\boldsymbol{k}\cdot\nabla T + \rho_0\boldsymbol{D}_X^v\cdot\nabla X + \rho_0\boldsymbol{D}_P^v\cdot\nabla P_g)\cdot\boldsymbol{n}_{ext} + \phi_h - \Delta h_v\phi_m = 0 \quad (21)$$

The third boundary condition expresses the fact that the total gas pressure is equal to atmospheric:

$$P_g = P_{atm} \quad (22)$$

Special attention must be paid to the case in which the interface is saturated and when liquid water can flow outside the medium due to overpressure inside the medium.

The numerical solution of the system uses the "TRANSPORE" code (Perré, 1987; Perré and Degiovanni, 1990; Perré and Moyne, 1991; Turner and Perré, 1995). The computation is based on the volume control method developed by Patankar (1980). Refer to these authors concerning the numerical aspect of the problem.

Total Liquid Saturation

The problem of total liquid saturation is easy to understand. In the model, since the liquid pressure is linked to the gas pressure through the capillary pressure, the disappearance of the gas phase makes it impossible to evaluate.

In fact, from a practical standpoint, when saturating a porous medium, it is very difficult to avoid trapping a small gas fraction in some pores. This suggests a solution to the numerical problem: a small fraction of the gas can be trapped if the gas flow vanishes just below full liquid saturation, that is, if the relative gas phase permeability vanishes at the so-called residual air saturation (Perré and Moyne, 1991).

This procedure is used to avoid the saturation of the inner volumes of the grid employed for the numerical discretization of the equations. As the liquid content approaches saturation, the pressure of the enclosed gas increases and the liquid pressure therefore increases, driving the liquid to a less saturated zone towards the surface.

A second rule is needed to decide when liquid expulsion occurs at the surface. Of course, if the liquid flow is weak, the thin liquid film at the interface can be removed by evaporation due to convective heat transfer. With a higher liquid flux, convective heat transfer is not sufficient. It is then necessary to define a criterion to evaluate the liquid flux at the interface illustrated by Figure 1. When liquid flows towards the surface, a numerical test compares the liquid pressure P_l (that is, to say the sum of the total gas phase pressure P_g and the capillary pressure P_c) of the next to last volume with the atmospheric pressure P_{atm}. If $P_l > P_{atm}$, the liquid flux entering the last volume flows directly outwards from the medium, corresponding to a liquid expulsion. If not, the normal procedure applies.

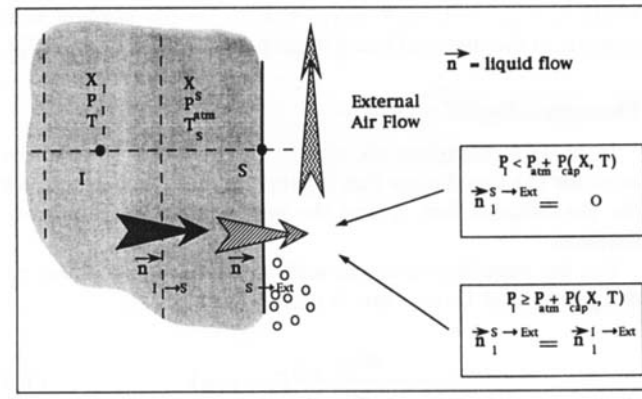

Figure 1. Numerical procedure at interface.

It would be very difficult to validate this approach through a drying experiment because of the large number of mechanisms involved. An isothermal drainage experiment with well-controlled boundary conditions was accordingly set up to compare experimental and numerical results. A vertical light concrete cylinder (height $h = 160$ mm; diameter $d = 40$ mm) was made impervious on its lateral surface by a resin coating reinforced by a glass fiber fabric. The cylinder, connected to a vacuum pump for several hours, was then saturated with deaerated water. The upper surface was covered with a 1-cm thick water film and the pressure was atmospheric. A constant air overpressure, not exceeding 10^4 Pa, was applied on the lower face. The second boundary condition necessary for the numerical simulation assumes that the lower surface is impervious to the total (liquid + vapor) water flux. The air flow through the lower face of the medium was measured by means of the pressure drop through a capillary tube. The mass of water expelled from the upper face was continuously recorded. The local liquid water saturation $S_l = \rho_0 X/\rho_l\epsilon$ (where ϵ is the porosity of the cylinder) was measured using gamma ray attenuation.

Figure 2a shows the average saturation $\bar{S}_l$ vs. time for slightly different values of the liquid migration coefficient D_X^l (defined in the annex) close to $S_l = 1$ depicted in Figure 2b. The result is very sensitive to this value, but relatively good agreement can be obtained. A more severe test of the model is shown in Figure 3, where the experimental and numerical saturation profiles vs. height are shown in steady-state condition. Agreement appears to be qualitatively good from the macroscopic standpoint.

The most intriguing aspect of this drainage experiment is the variation of the air flow entering the medium (Figure 4). After the initial transient period where the mass of expelled water and the air flux increase quickly, jumps appear in the air flow with time intervals of about 1 h, but the term "period" does not seem appropriate. The cycles observed can be broken down into three steps:

(1) A long stage with a very slow decrease in the air flux, which can be attributed to the filling of the porous medium by liquid water due to gravity and capillary forces.

(2) A fast air flux increase which intuitively corresponds to the opening of a new path for the air flux inside the

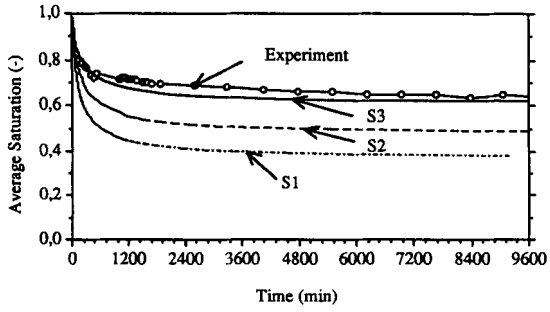

(a)

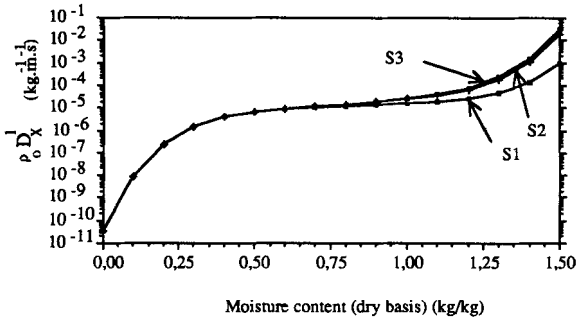

(b)

Figure 2. Drainage experiment: experimental and numerical average saturation vs. time (a); for different values of the liquid migration coefficient D_X^1(b).

medium. It is sometimes possible to observe the appearance of this new path on the upper face by examination of the exiting gas bubbles.

(3) A rapid air flux decrease to a value slightly higher than before the jump (this third step is not always observed), which corresponds to a quick reorganization of the air paths.

This occurrence is known as Haines jumps, and Morrow (1969) explains that the sudden jump at constant saturation arises from fluid interfaces which are unable to change curvature smoothly. The jumps (steps 1 and 3) are assumed to be irreversible whereas step 1 is reversible. Note here that the irreversible phase is responsible for the long-time increase of the air flux.

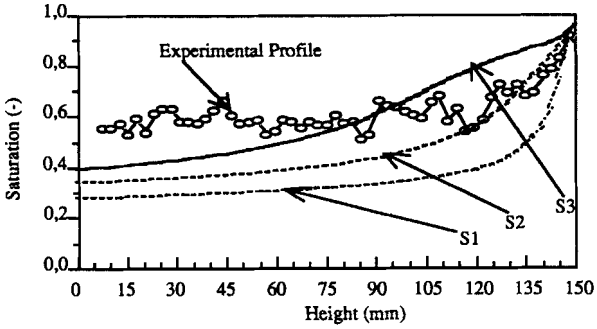

Figure 3. Drainage experiment: experimental and numerical saturation profiles in steady state.

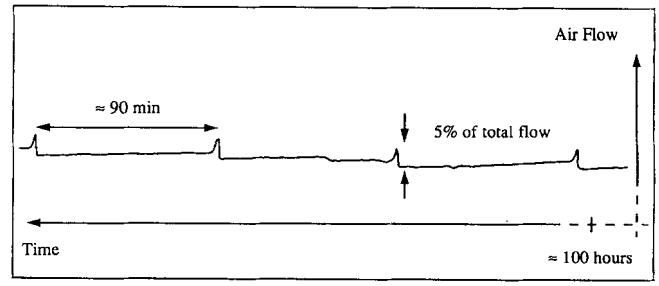

Figure 4. Drainage experiment: variation in air flow with time-Haines' jumps.

To conclude this section, even if the physics at the microscopic scale needs further explanations for the mechanisms encountered, the macroscopic description and the numerical procedure adopted here work very successfully and can be used with confidence to analyze liquid movements during microwave drying.

Microwave Drying

Experimental rig

The experimental rig is shown in Figure 5. The test section was a monomode rectangular wave-guide 160×90 mm, fed by a magnetron operating at 2.45 GHz. Power output was adjustable between 0 and 1kW.

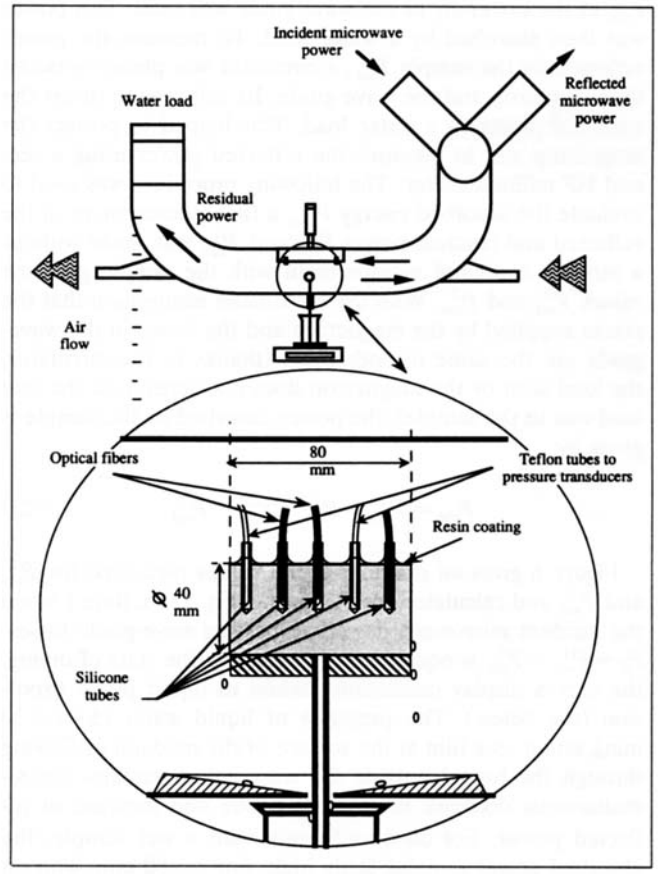

Figure 5. Microwave drying: experimental setup.

Aerothermal conditions were well-controlled by the succession of an electric fan, a condenser, a dehumidifier, a steam humidifier, and finally an electric heater. The experiments described here were conducted with an air temperature of 50°C, a low air relative humidity of 5%, and a gas velocity of about 1 $m \cdot s^{-1}$.

The sample were cylinders of light concrete (Ytong) (diameter: 40 mm; height: 80 mm) located transversally in the test section. They were made impervious on their lateral face with a resin coating. A number of silicone tubes were placed radially up to the center and glued. These tubes were used either to insert an optic fiber for temperature measurement, or Teflon capillaries filled with vaseline to avoid dead volumes, and joined to pressure transducers. The temperature was measured by the phosphorescence decay time constant. A previous calibration indicated that the temperature accuracy was about a few tenths °C. Accuracy of pressure measurement was tested up to an overpressure of one atmosphere by accurately checking the relation between temperature and saturated vapor pressure. All the materials used (silicone, teflon, vaseline) were chosen because they did not absorb microwave energy.

The drying sample was continuously weighed. A flat teflon funnel was cemented to the bottom face of the wave-guide to collect and to weigh the mass of expelled water.

Power dissipated

To measure the microwave energy absorbed by the product P_{abs}, an HF milliwattmeter that measures the residual power P_{res} at the extremity of the wave-guide was used. This power was then absorbed by a water load. To measure the power reflected by the sample P_{ref}, a circulator was placed between the magnetron and the wave-guide. Its role was to divert the reflected power to a water load. This helped to protect the magnetron and to measure the reflected power using a second HF milliwattmeter. The following procedure was used to evaluate the absorbed energy P_{abs}: a first measurement of the reflected and residual power P^1_{ref} and P^1_{res} was made without a sample. A second measurement with the sample gave the values P^2_{ref} and P^2_{res}. With the reasonable assumption that the power supplied by the magnetron and the losses in the wave-guide are the same in both cases (thanks to the circulator, the load seen by the magnetron does not depend on the real load due to the sample), the power absorbed by the sample is given by:

$$P_{abs} = P^1_{res} + P^1_{ref} - P^2_{res} - P^2_{ref} \tag{23}$$

Figure 6 gives an example of the values measured for P^2_{res} and P^2_{ref} and calculated for P_{abs} using. Eq. 23 vs. time t when the incident microwave power (neglecting wave-guide losses) $P_E = P^1_{res} + P^1_{ref}$ is equal to $P_E = 65$ W. At the start of drying, the curves display oscillations linked to liquid phase expulsion (see below). The presence of liquid water ($5 < t < 30$ min), either as a film at the surface of the medium or flowing through the funnel outside the wave-guide, explains the simultaneous decrease in residual power and increase in reflected power. For $30 < t < 50$ min with a wet sample, the absorbed power remains fairly high. For $t > 50$ min, with an increasingly dry sample, the absorbed power decreases as the

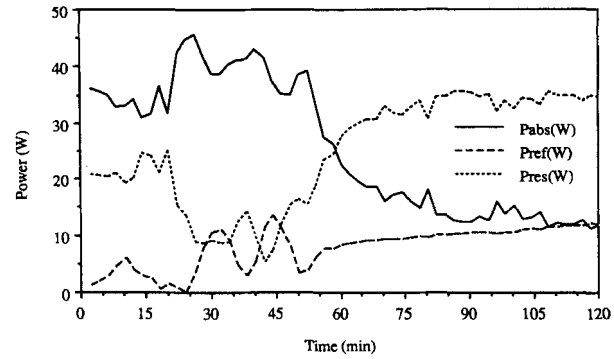

Figure 6. Absorbed (P_{abs}), reflected (P_{ref}) and residual (P_{res}) power ($P_E = 65$ W).

residual power increases to reach a nearly constant value at the end of drying.

Figure 7 shows the ratio of power dissipated in the medium per nominal power to the dry basis average moisture content of the sample. The similarity between the curves for various incident powers from 10 W to 160 W indicates that the average moisture content is of the utmost importance in the evaluation of dissipated power. Although a fairly accurate computation can be developed for a cylindrical body in a wave-guide (Pangrle et al., 1991), the experimental values P_{exp} of Figure 7 will be used in this study.

A simple but reasonable hypothesis is made to give the spatial distribution of the dissipated power per unit volume Φ assuming that:

$$\Phi = \frac{P_{exp}}{V} \frac{X^*}{\overline{X}^*} \tag{24}$$

where $X^* = \max(X_{hygr}, X)$. X_{hygr} is the upper limit of the hygroscopic range, $\overline{X}^*$ the average value of X^* over the sample and V the volume of the sample.

Formulation (Eq. 24) corresponds to a power preferentially dissipated in the wet zone, with a limited value in the hygroscopic range.

To compare the experimental results with the numerical results of a 1 – D computation along the height of the cylinder, the convective radial heat losses on the lateral surface of

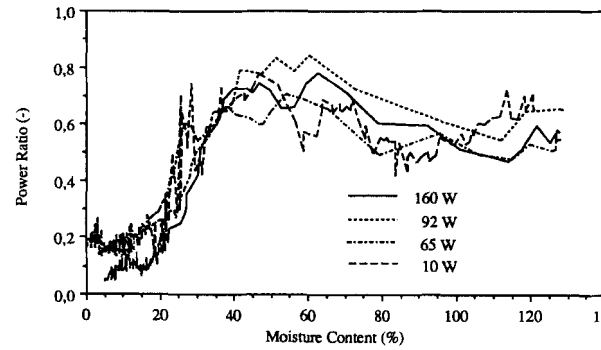

Figure 7. Power ratio (absorbed power)/(nominal power) vs. average moisture content for various nominal powers.

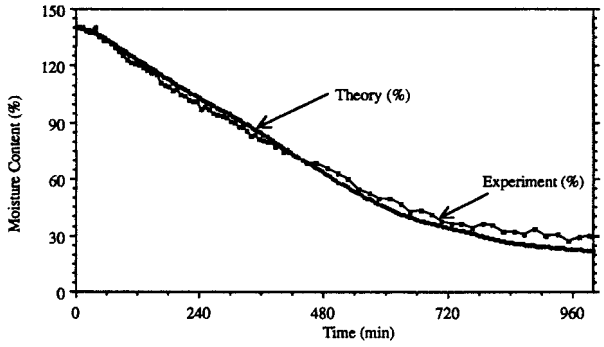

Figure 8. Experimental and numerical low power microwave drying kinetics ($P_E = 10$ W).

the sample must be added to Φ expressed in volumetric form. This assumption of a nearly uniform radial temperature is confirmed by a Biot number hR/k of about 0.2, where h is the external heat-transfer coefficient, R the radius of the cylinder and k its apparent thermal conductivity.

Low-power drying

Low-power drying refers to drying without boiling in the sample, that is, "low temperature" drying. For example, Figure 8 shows the experimental and numerical drying kinetics with an incident power $P_E = 10$ W. Agreement between experimental and numerical results is fairly satisfactory. This is not surprising, because drying is almost isenthalpic except for the sensible heat necessary to heat the medium and the convective heat losses. An examination of the numerical results in Figure 9 reveals a number of interesting aspects of microwave drying.

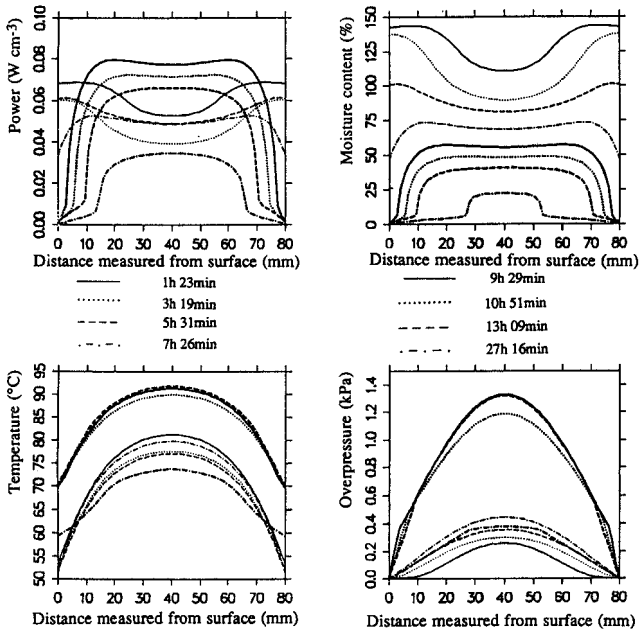

Figure 9. Numerical results: absorbed power, moisture content, temperature and gas overpressure profiles for low power microwave drying ($P_E = 10$ W).

After a warming up period, drying proceeds with a rather flat moisture content profile in the drying medium. Initially, the external zone of the sample is supplied with liquid water because of the low gas pressure gradient (due to a higher temperature and hence a higher saturated vapor pressure at the center) acting on the liquid phase, and because of the condensation of water vapor (which moves towards the surface with the temperature and gas pressure gradients as driving forces), due to the lower temperature of the ends of the cylinder. As the water mobility then decreases, the moisture content at the sample surface also decreases. A dry (in fact hygroscopic) zone recedes from the surface. Water transport through this zone is a combined gas phase convection-diffusion movement. The most interesting feature of low power microwave drying is the appearance of a favorable temperature gradient which, except in the final stage, serves to accelerate the drying rate significantly, without very steep moisture content profiles inside the medium. With low temperature, drying with internal heating allows for high drying rates. In convective drying, the driving force gradients of T and X oppose each other whereas in drying with internal heating, they act together, saving considerable time even with very low volume powers (Constant et al., 1992).

High power drying

Any understanding of microwave drying mechanisms at high power is based on the simultaneous examination of the experimental and numerical results concerning the drying kinetics (Figure 10), the temperature and gas pressure variations inside the sample (Figures 11 and 12), and the numerical profiles of absorbed power, temperature, moisture content and gas pressure (Figure 13) with an incident power $P_E = 65$ W. Agreement between the two results is good enough to allow a general description of the process using both results simultaneously.

Four periods can be distinguished:

(1) First, a short warming up period $0 < t < 7$ min where the temperatures rise quickly without significant mass losses. Microwave heating is, of course, very efficient.

(2) As the temperature rises, the internal gas pressure increases essentially through the saturated vapor pressure. The gas pressure then exceeds the atmospheric pressure gradient and pushes liquid water and vapor towards the surface. Since the temperature is lower at the surface than inside the material, vapor condenses. Due to the simultaneous liquid and gas

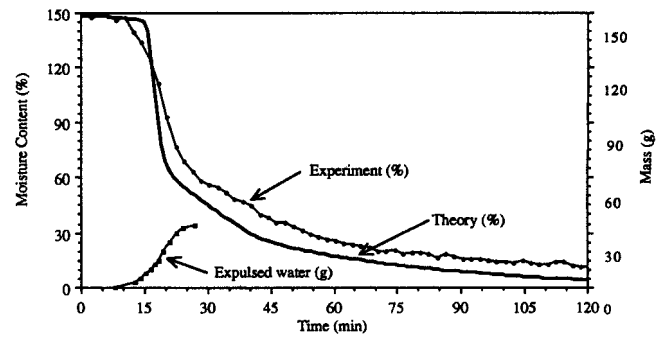

Figure 10. Experimental and numerical high power microwave drying kinetics ($P_E = 65$ W).

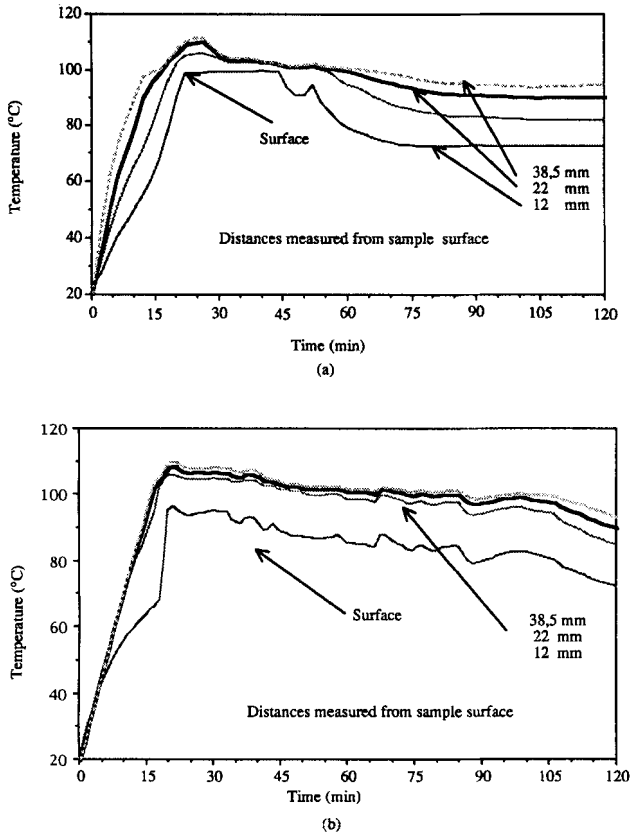

Figure 11. Experimental (a) and numerical (b) temperature variations during high power microwave drying ($P_E = 65$ W).

movement, a liquid plug forms at the ends of the sample and liquid expulsion begins. This period corresponds to a very steep slope of the mass curve vs. time. Since the sample surface is closed by the liquid plug, the temperature rises slightly above the boiling point of water and the gas pressure therefore increases with a maximum experimental overpressure of 50 kPa. From our experiments, it appears that the amount of water at the end of the liquid expulsion period does not vary significantly with absorbed power. For light concrete, nearly half the initial water content is expelled. This period ends

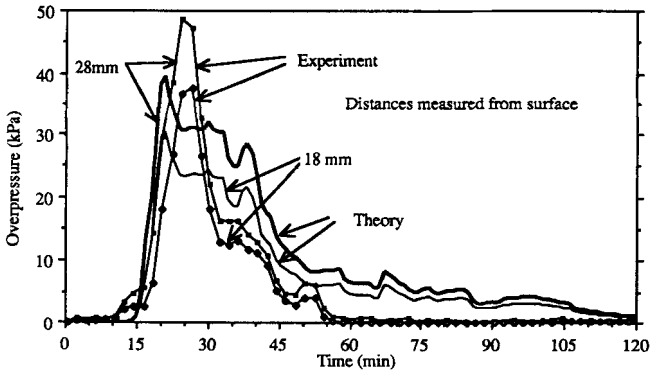

Figure 12. Experimental and numerical gas pressure variations during high power microwave drying ($P_E = 65$ W).

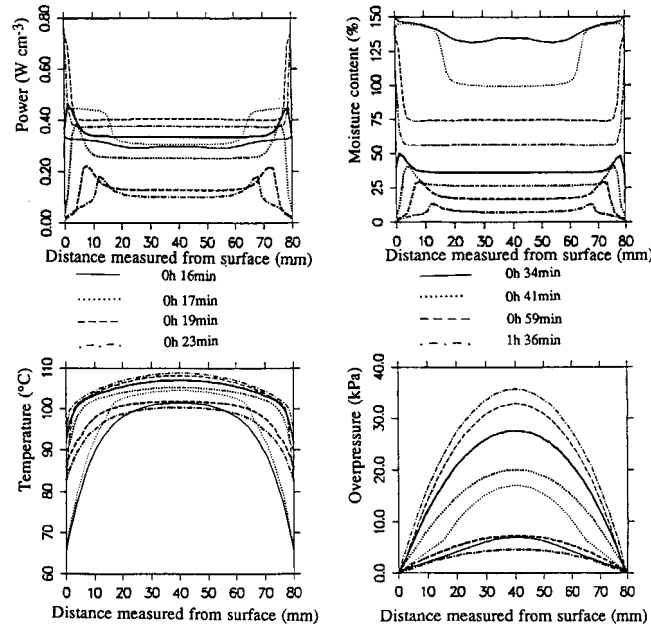

Figure 13. Numerical results: absorbed power, moisture content, temperature and gas overpressure profiles for high power microwave drying ($P_E = 65$ W).

when the liquid water mobility decreases with moisture content.

(3) In the third period, except for the convective heat losses, drying is isenthalpic. The absorbed power is used locally to evaporate water, which moves towards the surface under the influence of a favorable temperature and gas pressure gradient. As absorbed power and resistance to vapor transport decrease simultaneously, the temperature and gas pressure also decrease.

(4) In the final period, as the moisture content decreases a larger part of the energy is used by convective heat losses or to heat the medium. In Figures 10 to 13, due to the very low absorbed power at the end of the drying cycle, equilibrium is reached between microwave heating and convective losses by decreasing the temperatures; however, if power is increased, the temperature can rise sharply.

Conclusion

Microwave drying was investigated as a particular case of drying with internal heat generation. The heat source, that is, the absorbed microwave power, was determined experimentally and an ad hoc procedure was used in order to determine its spatial distribution.

The most convincing result of this study is the ability of the mathematical and numerical model to describe very satisfactorily the physical mechanisms of heat and mass transfer which occur during drying with internal heat generation. The classic distinction between "low temperature" and "high temperature" was observed, according to whether or not the temperature of the drying medium exceeded the boiling point imposed by the external pressure.

In "low temperature" drying, the acceleration of the drying

rate was explained by the simultaneous action of the temperature and moisture content gradients.

In "high temperature" drying, a thorough analysis of the liquid expulsion mechanisms was developed from both the experimental and numerical standpoints. Although the physics of the process at pore scale is rather complex, the simplified description retained at the macroscopic scale successfully explains the phase of liquid expulsion at the initiation of drying.

Notation

c_p = specific heat capacity, $J \cdot kg^{-1} \cdot K^{-1}$
D_v = binary air-vapor diffusion coefficient, $m^2 \cdot s^{-1}$
$\boldsymbol{D}$ = migration coefficient (see Appendix)
$\boldsymbol{f}$ = resistance tensor to gaseous diffusion
$\boldsymbol{g}$ = gravity intensity, $m \cdot s^{-2}$
h = specific enthalpy, $J \cdot kg^{-1}$
$\boldsymbol{j}$ = diffusive mass flux, $kg \cdot m^{-2} \cdot s^{-1}$
$\boldsymbol{k}$ = apparent thermal conductivity, $W \cdot m^{-1} K^{-1}$
$\boldsymbol{k}_r$ = relative permeability
$\boldsymbol{K}$ = intrinsic permeability, m^2
$\dot{m}$ = mass of evaporated water per unit volume and per unit time, $kg \cdot m^{-3} \cdot s^{-1}$
M = molar mass, $kg \cdot mol^{-1}$
$\boldsymbol{n}$ = mass flux density, $kg \cdot m^{-2} \cdot s^{-1}$
$\boldsymbol{n}_{ext}$ = normal to the surface (outwardly directed)
P = pressure, Pa
P_E = electromagnetic power, W
$\boldsymbol{q}$ = heat flux density, $W \cdot m^{-2} \cdot K^{-1}$
R = gas constant, $J \cdot mol^{-1} \cdot K^{-1}$
S = saturation
t = time, s
T = temperature, K
$\boldsymbol{u}$ = superficial velocity, $m \cdot s^{-1}$
V = volume, m^3
X = moisture content (dry basis)

Greek letters

α, β, γ = coefficients (see Eq. 18 and Appendix)
ϵ = porosity
Δh_v = latent heat of vaporization, $J \cdot kg^{-1}$
λ = thermal conductivity, $W \cdot m^{-1} K^{-1}$
μ = dynamic viscosity, $kg \cdot m^{-1} \cdot s^{-1}$
ρ = density, $kg \cdot m^{-3}$
ϕ = surface flux density
Φ = volume heat source, $W \cdot m^{-3}$
φ = air relative humidity

Subscripts and superscripts

a = air
exp = experimental
G = relative to gravity
h = heat
l = liquid
P = relative to P
s = solid
T = relative to T
vs = saturated vapor
X = relative to X
0 = dry
$\bar{}$ = average value

Literature Cited

Azizi, S., C. Moyne, and A. Degiovanni, "Approche Expérimentale et Théorique de la Conductivité Thermique des Milieux Poreux Humides: I. Expérimentation," *Int. J. Heat Mass Transf.*, **31**, 2305 (1988).

Constant, T., "Le Séchage Combiné Convection-Micro-Ondes: Modélisation, Validation, Optimisation," PhD Thesis, INPL, Nancy, France (1992).

Constant, T., P. Perré, and C. Moyne, "Microwave Drying of Light Concrete: from Transport Mechanisms to Explanation of Energy Savings," *Drying '92*, A.S. Mujumdar, ed., Elsevier Science Publishers B. V., p. 617 (1992).

Dullien, F. A. L., *Porous Media—Fluid Transport and Pore Structure*, 2nd ed., Academic Press Inc., San Diego, CA (1992).

Jolly, P., and I. W. Turner, "Combined Microwave Drying of a Porous Material," *Drying Technol.*, **9**, 1209 (1991).

Lefeuvre, S., B. Mangin, B. and Y. Rezvan, "Industrial Materials Drying by Microwave and Hot Air," *IMPI Microwave Power Symp.*, Ottawa, ONT, p. 65 (June 28–30, 1978).

Lyons, D. W., J. D. Hatcher, and J. E. Sunderland, "Drying of a Porous Medium with Internal Heat Generation," *Int. J. Heat Mass Transf.*, **15**, 897 (1972).

Metaxas, A. C., and R. J. Meredith, "Industrial Microwave Heating," *IEE Power Eng. Ser. 4*, Peter Peregrinus Ltd, London (1988).

Morrow, N. R., "Physics and Thermodynamics of Capillary," *Symp. Flow through Porous Media*, The Carnegie Institution, Washington, DC (June 9–11, 1969).

Morrow, R., "Applications of Radio-Frequency Power to the Drying of Timber," *IEE Proc.*, **27** A(6)(1980).

Moyne, C., "Transferts Couplés Chaleur-Masse lors du Séchage: Prise en Compte du Mouvement de la Phase Gazeuse," PhD Thesis, INPL, Nancy, France (1987).

Moyne, C., J. C. Batsale, and A.Degiovanni, "Approche Expérimentale et Théorique de la Conductivité Thermique des Milieux Poreux Humides: II. Théorie," *Int. J. Heat Mass Transfer*, **31**, 2319 (1988).

Moyne, C., and P. Perré, "Processes Related to Drying: I. Theoretical Model," *Drying Technol.*, **9**, 1135 (1991).

Pangrle, B. J., K. G. Ayappa, H. T. Davis, E. A. Davis, and J. Gordon, "Microwave Thawing of Cylinders," *AIChE J.*, **37**, 1789 (1991).

Patankar, S. V., *Numerical Heat Transfer and Fluid Flow*, Hemisphere Publishing, New York (1980).

Perré, P., "Le Séchage Convectif de Bois Résineux: Choix, Validation et Utilisation d'un Modèle," PhD Thesis, Univ. de Paris VII, France (1987).

Perré, P., and A. Degiovanni, "Simulation par Volumes Finis des Transferts Couplés de Chaleur et de Masse en Milieux Poreux Insaturés Anisotropes: Séchage du Bois à Basse et Haute Température," *Int. J. Heat Mass Transf.*, **33**, 2463 (1990).

Perré, P., and C. Moyne, "Processes Related to Drying: II. Use of the Same Model to Solve Transfers both in Saturated and Unsaturated Media," *Drying Technol.*, **9**, 1153 (1991).

Perré, P., and I. W. Turner, "A Comparison of the Drying Simulation Codes TRANSPORE and WOOD2D which are used for the Modelling of Two-Dimensional Drying Processes," *Drying Technol.*, **13**, 695 (1995).

Whitaker, S., "Simultaneous Heat, Mass, Momentum Transfer in Porous Media: A Theory of Drying," *Adv. in Heat Transf.*, **13**, 119 (1977).

Appendix: Coefficients of the Model

$$D_X^1 = -\frac{\rho_1}{\rho_0}\frac{Kk_{rl}}{\mu_1}\left(\frac{\partial P_c}{\partial X}\right)_T$$

$$D_T^1 = -\frac{\rho_1}{\rho_0}\frac{Kk_{rl}}{\mu_1}\left(\frac{\partial P_c}{\partial T}\right)_X$$

$$D_P^1 = \frac{\rho_1}{\rho_0}\frac{Kk_{rl}}{\mu_1}$$

$$D_G^1 = \frac{\rho_1}{\rho_0}\frac{Kk_{rl}}{\mu_1}\rho_1$$

$$D_x^v = \frac{1}{\rho_0}\frac{D_v}{RT}f\frac{M_a M_v}{M}\left(\frac{\partial p_v}{\partial X}\right)_T$$

$$D_T^v = \frac{1}{\rho_0}\frac{D_v}{RT} f \frac{M_a M_v}{M}\left(\frac{\partial p_v}{\partial T}\right)_X$$

$$D_P^v = -\frac{\rho_v}{\rho_0}\frac{Kk_{rg}}{\mu_g} - \frac{1}{\rho_0}\frac{D_v}{RT} f \frac{M_a M_v}{M}\frac{P_v}{P}$$

$$D_G^v = \frac{\rho_v}{\rho_0}\frac{Kk_{rg}}{\mu_g}\rho_g \cong 0$$

$$D_P^a = \frac{\rho_a}{\rho_0}\frac{Kk_{rg}}{\mu_g} + \frac{1}{\rho_0}\frac{D_v}{RT} f \frac{M_a M_v}{M}\frac{P_v}{P}$$

$$k = \lambda + \rho_0 \Delta h_v D_T^v$$

$$\alpha = \frac{\epsilon M_a (1 - S_1)}{\rho_0 RT}$$

$$\beta = -\frac{\epsilon M_a (1 - S_1)}{\rho_0 RT}\left[\left(\frac{\partial p_v}{\partial X}\right)_T + \rho_0 \frac{P_g - P_v}{\rho_1 \epsilon (1 - S_1)}\right]$$

$$\gamma = -\frac{\epsilon M_a (1 - S_1)}{\rho_0 RT}\left[\left(\frac{\partial p_v}{\partial T}\right)_X + \frac{P_g - P_v}{T}\right]$$

with

$$S_1 = \frac{\rho_0 X}{\rho_1 \epsilon}$$

Manuscript received Oct. 17, 1994, and revision received Feb. 27, 1995.